Journal of Photochemistry and Photobiology A: Chemistry 216 (2010) 209–214

Contents lists available at ScienceDirect

Journal of Photochemistry and Photobiology A: Chemistry

journal homepage: www.elsevier.com/locate/jphotochem

# Synthesis and characterisation of Fe–V–O thin film photoanodes

Craig D. Morton, Ian J. Slipper, Michael J.K. Thomas, Bruce D. Alexander*

*University of Greenwich, School of Science, Central Avenue, Chatham Maritime, Kent ME4 4TB, United Kingdom*

ARTICLE INFO

*Article history:*
Available online 19 August 2010

*Keywords:*
Photocatalysis
Semiconductor
Raman spectroscopy
Thin films
Electrodes
Hydrogen

ABSTRACT

$FeVO_4$ was synthesised using a low temperature, aqueous precipitation reaction. The material prepared directly from this synthesis was found to be predominantly amorphous and required a thermal treatment. The resultant material was characterised using XRD, FT-IR, Raman spectroscopy and magnetic susceptibility measurements. Materials annealed above 600 °C were found to consist mainly of $FeVO_4$, although traces of hematite were found following annealing at higher temperatures. Diffuse-reflectance UV spectroscopy and subsequent Tauc plots revealed a band gap of *ca.* 2.00 eV corresponding to an indirect transition. Photocurrent–voltage characteristics recorded under simulated solar illumination indicate that photocurrents are sensitive to annealing temperature and the number of layers deposited on an electrode surface.



## 1. Introduction

It has been estimated that global energy consumption will reach almost 27 TW by 2050 [1]: the majority of this demand will be met by fossil fuels [2]. The development of new non-polluting energy sources is therefore desirable. A move towards a hydrogen economy has in part been hindered by the development of sustainable means of hydrogen production to replace steam reformation of natural gas. Solar hydrogen production through the use of semiconductor photocatalysts to split water into oxygen and hydrogen has attracted a great deal of interest since its discovery by Fujishima and Honda [3]. Numerous photocatalytically, and photoelectrocatalytically active materials have been reported although the widest studied remains $TiO_2$ [4]. However, $TiO_2$ has a comparatively large band gap (*ca.* 3.1 eV) which implies that the useful conversion of solar radiation is limited to 4% of photons which reach the surface of the Earth [5]. There is therefore a need to develop photo(electro)catalysts which have smaller band gaps, and are thus active to visible light, such as tungsten trioxide or iron oxide [6–8]. Tungsten trioxide has been shown to be active towards visible light, with a band gap of 2.5 eV. Nevertheless, a further reduction in band gap is desirable, hence the interest in developing iron oxide for photocatalysis. However, iron oxide suffers from losses associated to fast electron–hole recombination [5]. Another way of shortening the band gap compared to binary oxides has prompted reports of the photocatalytic properties of bismuth vanadate [9–11] and indium vanadate [12]. In the case of $BiVO_4$ (band gap of 2.4 eV), the Bi 6s orbitals are thought to hybridize with O 2p orbitals, thereby shifting the valence band to a more negative potential [9]. The use of iron rather than bismuth should further lower the band gap whilst avoiding the use of precious metals such as indium. Furthermore, a combinatorial study on iron based binary oxides suggested that iron vanadate was expected to be a photoelectrocatalytically active material [13]. Iron vanadate has already been investigated in other catalytic studies, such as for the oxidation of hydrocarbons [14] and in the degradation of orange II [15] although it should be stressed that neither of these reports concern the use of photocatalysis. In this communication, we report the synthesis and characterisation of iron vanadate thin film electrodes and the result of initial photoelectrochemical analysis.

## 2. Experimental

Iron vanadate powders were prepared following a low-temperature aqueous precipitation reaction [16]. Equimolar aqueous solutions of ammonium metavanadate (99%, Alfa Aesar) and iron nitrate nonahydrate (98–100%, Riedel-de Haën) were introduced into a closed, sealed vessel and heated to 70 °C for 72 h. The resulting orange suspension was centrifuged, washed with acetone and water before being dried in an oven at 50 °C to obtain an orange-brown solid. For analysis of the effect of annealing, the dried powder was then annealed at a range of temperatures between 250 and 700 °C and in air, oxygen and nitrogen. Electrodes were prepared by drop-coating a suspension of un-annealed iron vanadate

* Corresponding author. Tel.: +44 208 3318209.
*E-mail address:* B.Alexander@greenwich.ac.uk (B.D. Alexander).

1010-6030/$ – see front matter © 2010 Elsevier B.V. All rights reserved.
doi:10.1016/j.jphotochem.2010.08.010

in DMF/PVDF onto glass electrodes with an F-doped $SnO_2$ overlayer (Solaronix, CH). One layer was made following the deposition of the suspension onto the conducting glass substrate, which was then dried in air at room temperature for 10 min and the excess material removed by the doctor-blading technique. The electrode was then annealed at a given temperature between 250 and 700 °C, typically for 10 min in oxygen atmosphere. This process was repeated to deposit additional layers (*e.g.* 3 or 6 layers) of approximately 2.0 cm × 1.0 cm in dimensions.

X-ray diffraction (XRD) measurements were recorded using Siemens D500 diffractometer with a Cu anode at 40 kV and 40 mA, 1° divergent and receiving slits, 0.15° detector slit, a scintillation counter at a speed of 1° $2\theta$ per minute; a graphite monochromator was used to remove $CuK_\beta$ radiation. Scanning electron microscopy (SEM) was performed using a Cambridge Instruments Stereoscan 360 at an accelerating voltage of 30 kV, and a working distance 4 mm. Secondary electron images were collected from samples sputter coated in gold (2 min at 1 kV, 30 mA, Edwards S150B). Infrared spectra were recorded from pressed KBr discs on a Paragon 1000 FT-IR spectrometer (Perkin Elmer). Powders were analysed by Raman microscopy using a LabRam I Raman microscope (Horiba Jobin Yvon) fitted with a CCD camera and an Olympus microscope. Spectra were recorded using 532 nm laser illumination from a frequency-doubled Nd:YAG laser and a 100× objective. Optical band gaps were estimated from diffuse reflectance UV/Vis spectroscopy recorded on a Jasco V-650 spectrometer. Spectralon was used as a reference material.

For the photoelectrochemical measurements, samples were placed in 0.5 M NaOH in a custom-made Teflon cell, fitted with a quartz window. The counter electrode was a platinum sheet and the reference electrode was a saturated calomel electrode. Samples were irradiated from the solution–semiconductor interface by simulated solar irradiation from a 150 W Xe lamp (Oriel, 6253) housed in an Oriel 66907, fitted with AM1.5 and IR filters. AM1.5 filters are designed to provide standard illumination that simulates solar irradiation. The light intensity measured at the sample using Newport 818P thermopile sensor attached to a Newport 1918-C Hand-Held Optical Power meter was 100 mW $cm^{-2}$. A microAutolabIII potentiostat was used for all electrochemical measurements.

## 3. Results and discussion

To estimate the thickness of the deposited films, an electrode that consisted of 6 layers annealed at 650 °C in nitrogen was cut in half and the edge of the electrode was analysed by SEM and EDX. The thickness of these electrodes was found to be around 500 nm. Fig. 1 shows SEM micrographs obtained from powders annealed at 250 and 650 °C (Fig. 1a and b, respectively) and a typical electrode annealed at 650 °C (Fig. 1c).

After annealing at 250 °C, particles are typically rough spherical particles in the 50–80 nm range. Increasing the annealing temperature produces smoother particles that are around 100 nm in diameter. Micrographs of the surface of the thin-film electrodes annealed at 650 °C reveal particles of a similar size to those of the powder. However, it should be noted that the appearance of prismatic particles is now observed. Fig. 1c suggests that the films have a significant degree of porosity, which should easily allow penetration of the electrolyte.

XRD diffractograms, given in supplementary information, indicate a clear increase in crystallinity when the iron vanadate powders are annealed at higher temperatures, in particular those annealed above 450 °C which showed clearly visible features. For samples annealed above 600 °C the crystallinity increased markedly and clearly resolved peaks could be assigned to triclinic $FeVO_4$ by comparison with the International Centre for Diffraction

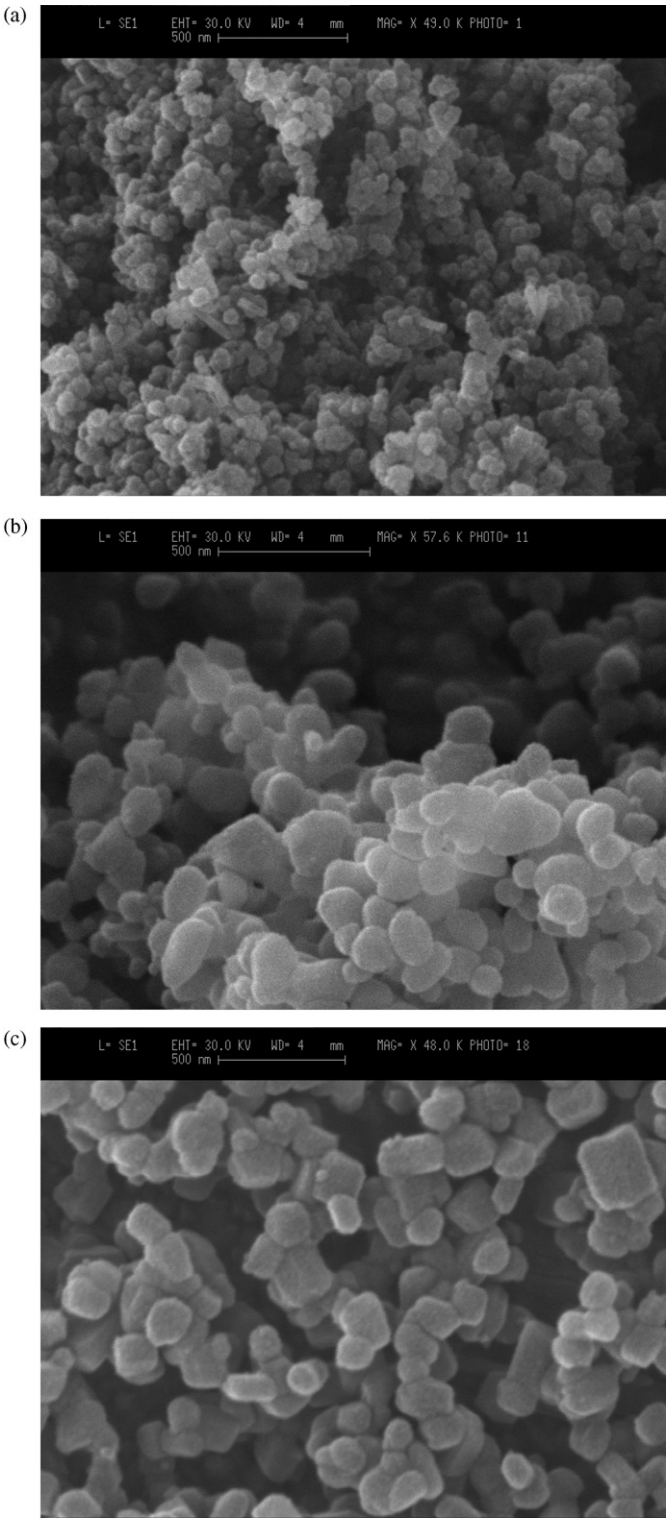


**Fig. 1.** SEM images of powder annealed at: (a) 250 °C; (b) 650 °C and (c) electrode annealed at 650 °C.

Data (ICDD) pattern no. 038-1372. A small amount of hematite ($\alpha$-$Fe_2O_3$) was indicated by peaks at 24.15°, 33.17°, 35.63°, 49.5°, and 54.08° $2\theta$ (ICDD pattern no. 033-0664) was also present, as indicated by an asterisk. XRD diffraction patterns were also recorded for the iron vanadate thin films *in situ* on the electrode surfaces, these are given in Fig. 2. The most intense peaks are predominantly due to the conducting glass electrode (*e.g.* $SnO_2$) upon which the iron vanadate is deposited. The strongest iron vanadate peaks

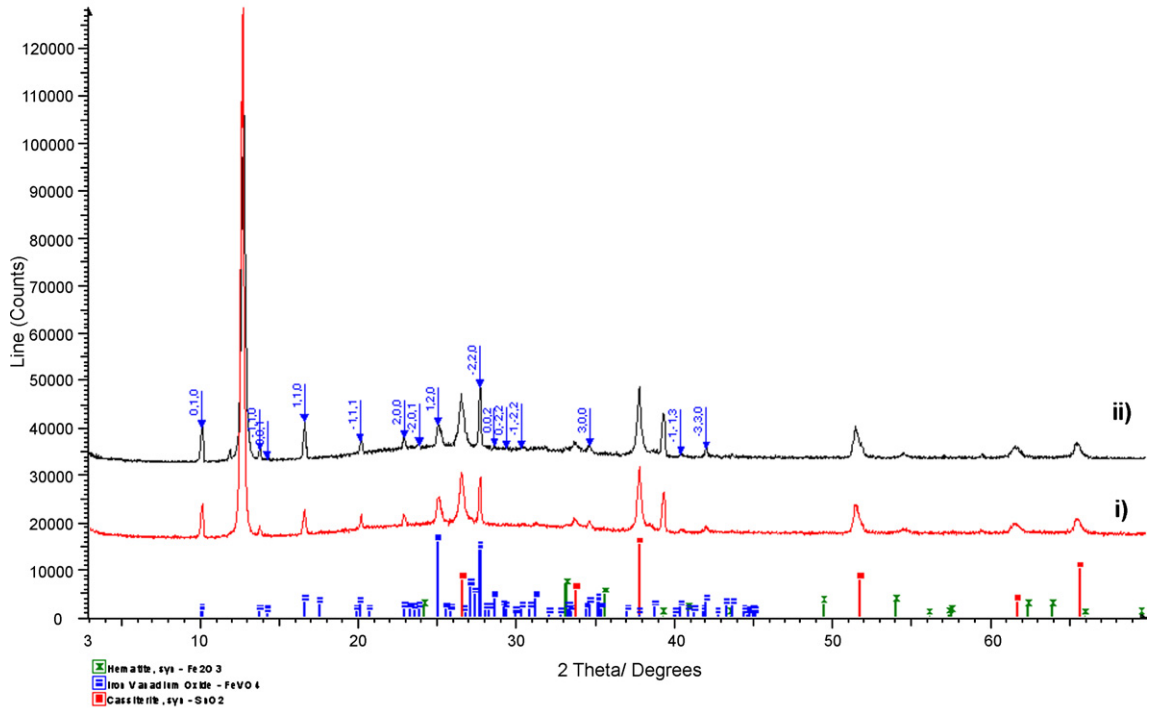


**Fig. 2.** XRD of iron vanadate thin films consisting of 6 layers annealed at 650 °C in (i) nitrogen and (ii) oxygen.

are occur at 10.1°, 16.6°, 20.1° 25.0° and 27.8° $2\theta$. These correspond to the [0,1,0], [1,1,0], [−1,1,1], [1.2.0] and [−2,2,0] crystal planes, respectively. Diffraction patterns obtained from electrodes annealed below 550 °C, or those that consisted of three layers showed only cassiterite and are therefore not reported. No effect of annealing atmosphere was observed on the diffraction patterns.

Infrared spectra for samples annealed in air are shown in Fig. 3. The spectra resulting from samples annealed below 350 °C display broad, ill-defined features below 1000 $cm^{-1}$, typical of amorphous material. In a similar trend to that observed in the XRD data (supporting information), the infrared spectra show sharper, better-defined bands as the annealing temperature increases. The increased resolution of bands around 700, 800 and 950 $cm^{-1}$ indicate that samples annealed between 450 and 550 °C show the onset of crystallisation. This crystallisation is apparently complete for samples annealed above 650 °C. Clearly defined bands *ca.* 950 $cm^{-1}$ corresponding to $VO_4$ tetrahedra are observed along with bands in the 710–740 $cm^{-1}$ region that correspond to Fe–O stretches for $Fe^{3+}$ atoms surrounded by oxygen atoms in square pyramidal and octahedral arrangements [17] that are expected to be present in the triclinic phase of iron vanadate [18].

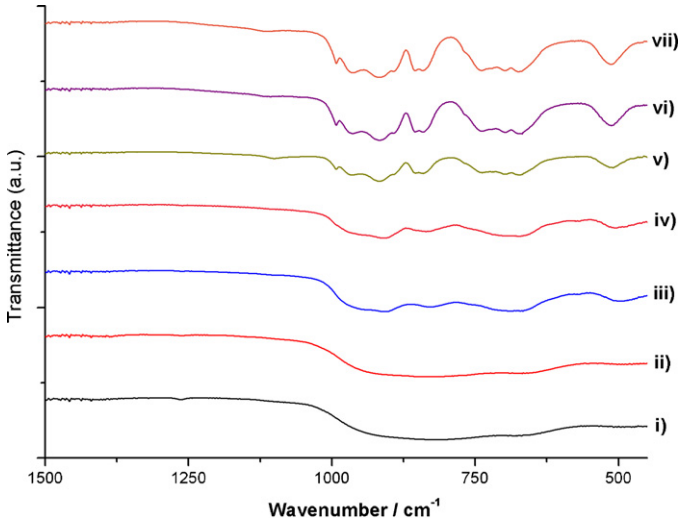


**Fig. 3.** IR spectra of iron vanadate powders annealed in air at: (i) 250 °C; (ii) 350 °C; (iii) 450 °C; (iv) 550 °C; (v) 600 °C; (vi) 650 °C; and (vii) 700 °C.

Raman microscopy enabled the facile analysis of the iron vanadate thin films, as deposited on the electrode surfaces, shown in Fig. 4, and consolidated the interpretation of the infrared and XRD analysis.

Similar to the previous spectroscopic analysis, samples annealed below 350 °C indicated a material that was mostly amorphous, as evidenced by the weak, broad features in the Raman spectra. Interestingly, in contrast to the data obtained for powder samples, the material deposited on electrodes appears to remain largely amorphous after annealing at 450 °C. It is not until electrodes are annealed at 550 °C that bands start to become better resolved. A summary of band positions and assignments is given in Table 1. Bands around 750, 825 and 920 $cm^{-1}$ appear in the Raman spectra of films annealed at 550 °C. Li et al. observed a band at 827 $cm^{-1}$ in the Raman spectra of $BiVO_4$ [11]. This was assigned to V–O symmetric stretching vibrations in $VO_4$ tetrahedra. The band present *ca.* 750 $cm^{-1}$ is tentatively assigned to an asymmetric V–O stretch [19]. Vuk et al. proposed that these bands present in $FeVO_4$ to be due to bridging V–O–Fe stretching modes [20]. The V–O–V deformations are just perceptible in very weak features around 400 and 450 $cm^{-1}$. Annealing the electrodes at 600 °C afforded a marked increase in the strength of the Raman spectrum obtained. A larger number of bands became readily observed and could be easily resolved, in particular below 600 $cm^{-1}$, reflecting the increase in crystallinity of the layer. The spectra of the samples annealed above 600 °C agree well with the results observed by Vuk et al. [20]. The bands present in the electrode annealed at 550 °C split into at least two bands when the annealing temperature is raised to 600 °C, reflect-

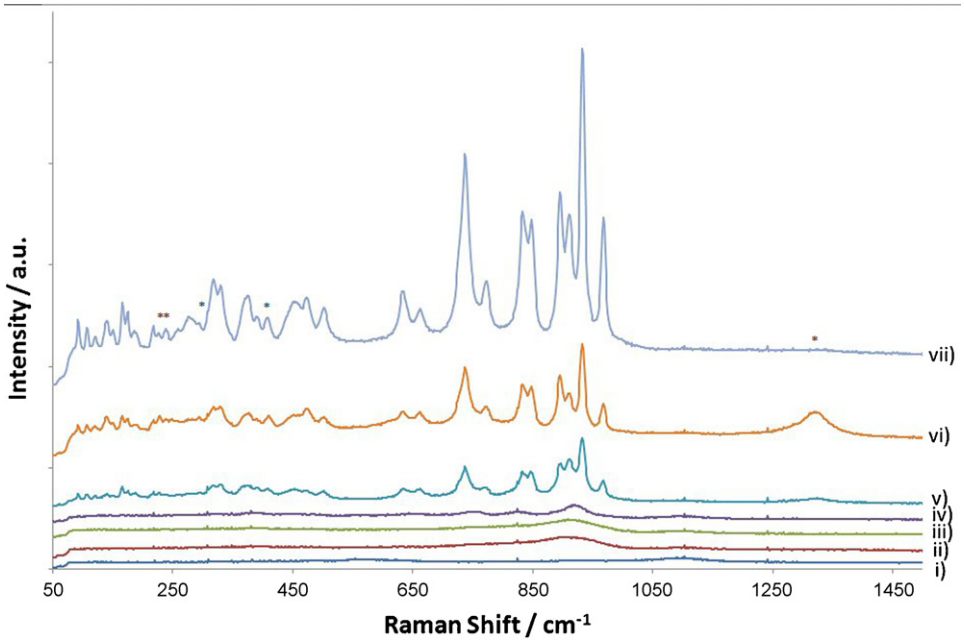


**Fig. 4.** Raman spectra of iron vanadate electrodes annealed in air at: (i) 250 °C; (ii) 350 °C; (iii) 450 °C; (iv) 550 °C; (v) 600 °C; (vi) 650 °C; and (vii) 700 °C. Excitation wavelength = 532 nm. * shows the position of bands that could be assigned to hematite.

ing the formation of triclinic $FeVO_4$. The bands can be grouped into three regions: 700–800; 800–900; and 900–1000 $cm^{-1}$. These regions correspond to V–O stretching modes involving bridging oxygen atoms. As the O–Fe interactions increase, the corresponding Raman band decreases in Raman shift. For example, the two bands at 635 and 667 $cm^{-1}$ correspond to Fe–O stretching vibrations in $FeO_5$ distorted trigonal bipyramids and $FeO_6$ octahedra [17]. Below 550 $cm^{-1}$, bands due to deformations are clearly discernible. Bands present between 300 and 400 $cm^{-1}$ in the infrared spectra of $Fe_{3-x}V_xO_4$ powders were assigned to O–V–O deformations [21]. It is therefore suggested that the medium intensity bands at 330 and 373 $cm^{-1}$ arise from similar modes of vibration. In the Raman spectrum of the electrode annealed at 600 °C, the bands can be assigned to $FeVO_4$ with one exception: there is a broad, weak band centred around 1323 $cm^{-1}$. This band is due to the second-order magnon band of hematite [22]. Further evidence for this assignment is provided by the fact that the intensity of this band is critically depended on the excitation wavelength and is not observed when the excitation wavelength is changed to 633 nm. There is no evidence for hematite in the Raman spectra of samples annealed below 550 °C. For the most part, the quantity of hematite is expected to be low, given that this second-order scattering can

**Table 1**
Summary of Raman band positions (in $cm^{-1}$) and assignments.

| Annealing temperature (°C) | | | | Assignment | Species | Reference |
|---|---|---|---|---|---|---|
| 350 | 450 | 550 | 600–700 | | | |
| | | | 1323 | 2nd order magnon | $\alpha$-$Fe_2O_3$ | [22] |
| | | | 969 | Terminal V–O stretch | $FeVO_4$ | [20] |
| | | | 932 | Terminal V–O stretch | $FeVO_4$ | [20] |
| 901 | 909 | 915 | 911 | Terminal V–O stretch | $FeVO_4$ | [20] |
| | | | 896 | Terminal V–O stretch | $FeVO_4$ | [20] |
| | | | 848 | Bridging V–O–Fe stretch | $FeVO_4$ | [20] |
| | | | 933 | Bridging V–O–Fe stretch | $FeVO_4$ | [20] |
| | | 823 | | $VO_4$ symmetric stretch | $FeVO_4$ | [11] |
| | | | 772 | Bridging V–O–Fe stretch | $FeVO_4$ | [20] |
| | 751 | 748 | | $VO_4$ asymmetric stretch | $FeVO_4$ | [20] |
| | | | 738 | Bridging V–O–Fe stretch | $FeVO_4$ | [20] |
| | | | 661 | $FeO_5$/$FeO_6$ stretch | $FeVO_4$ | [17,20] |
| | | | 633 | $FeO_5$/$FeO_6$ stretch | $FeVO_4$ | [17,20] |
| | | | 501 | | | |
| | | | 472 | | | |
| | | | 450 | V–O–V deformation | $FeVO_4$ | [20] |
| | | | 406 | V–O–V deformation | $FeVO_4$ | [20] |
| | | | 383 | | $\alpha$-$Fe_2O_3$ | [22] |
| | | | 373 | O–V–O deformation | $FeVO_4$ | [21] |
| | | | 330 | O–V–O deformation | $FeVO_4$ | [21] |
| | | | 318 | | | |
| | | | 284 | | $\alpha$-$Fe_2O_3$ | [22] |
| | | | 270 | | | |
| | | | 257 | | | |
| | | | 236 | | $\alpha$-$Fe_2O_3$ | [22] |
| | | | 225 | | $\alpha$-$Fe_2O_3$ | [22] |
| | | | 215 | | | |

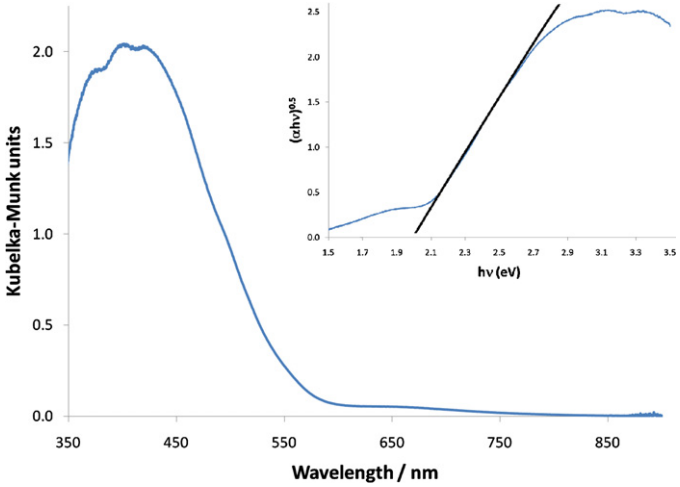


**Fig. 5.** Diffuse reflectance spectrum for an iron vanadate electrode annealed in oxygen at 650 °C. Inset: Tauc plot for the same electrodes.

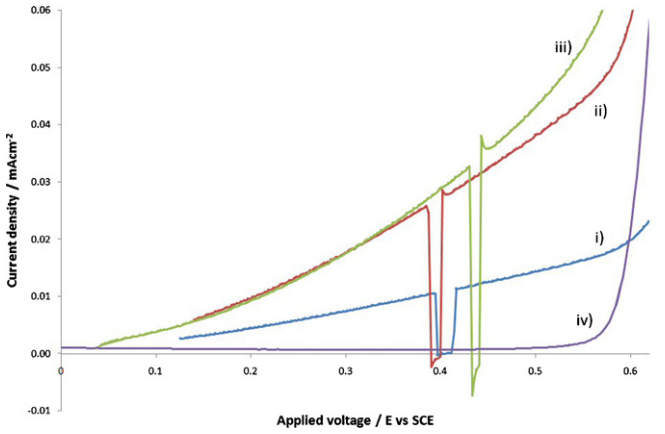


**Fig. 6.** Photocurrent–voltage plots for iron vanadate electrodes annealed for 10 min per layer at 550 °C. Electrodes contain: (i) 1 layer; (ii) 3 layers; and (iii) 6 layers. Sudden drops in photocurrent density between 0.38 and 0.45 V occurred when the AM1.5 light was switched off. The corresponding dark current is given in (iv).

afford a very intense band in thin films of iron oxide electrodes [7]. Other peaks that are potentially attributable to hematite are labelled with an asterisk in Fig. 4, although it should be stressed that these are weak and generally obscured by stronger features that have been assigned to iron vanadate.

An estimation of optical band gap can be gained from diffuse reflectance UV/Vis spectroscopy following conversion of the spectra into Kubelka–Munk units [23]:

$$F(R) = \frac{(1-R)^2}{2R} \quad (1)$$

where $R$ is the reflectance. Fig. 5 shows a typical reflectance spectrum for an electrode formed after annealing in an oxygen atmosphere.

There is substantial absorbance up to *ca.* 600 nm and a weak secondary feature appears around 650 nm. Further information can be determined through application of this data to the Tauc equation [24]:

$$\alpha h\nu = A(h\nu - E_g)^n \quad (2)$$

where $A$ is the proportionality constant, $\alpha$ is the absorption coefficient, $\nu$ is the frequency of light and $E_g$ is the band gap. The value of $n$ is dependent on the nature of the transition: $n$ is 1/2 for a directly allowed transition and 2 for an indirectly allowed transition [25,26].

The inset of Fig. 5 shows the resulting Tauc plot, which is linear over a greater range of photon energies than that which corresponds to a direct transition (given in supporting information). Here, $n = 2$ gave a linear fit indicating that the band gap corresponds to an indirect optical transition. This is in agreement with experimental observations for $BiVO_4$ [11], although it should be noted that Dunkle et al. concluded that $BiVO_4$ had a direct band gap transition based on DFT calculations [10]. Similar calculations are required to fully ascertain the nature of the bands present in $FeVO_4$, and indeed the exact nature of the optical transition. From the Tauc plot, it is possible to estimate the band gap energy. This has been found to be *ca.* 2.00 eV for the present samples.

A series of electrodes were prepared by depositing 1, 3 and 6 layers of iron vanadate and annealing each layer for 10 min at 550 °C in flowing oxygen. The photocurrent-potential characteristics were recorded upon exposure of the electrodes to simulated AM1.5 light.

The resulting data are shown in Fig. 6, the drop in photocurrent indicates where the light has been chopped and thus corresponds to dark current. Typical dark current for these electrodes is shown in Fig. 6(iv). Although the photocurrents are small, 50 μA cm$^{-2}$ at best (at 0.53 V *vs.* SCE), there is a measurable photocurrent even with comparatively poorly crystalline materials as indicated by Raman microscopy. One might suspect that such a photocurrent arises from the presence of iron oxide in the film [6,7,27], however it is to be recalled that no $Fe_2O_3$ was detected in the Raman analysis, nor the XRD data given above. Initial results indicate that the photocurrent increases as the number of layers increases, thereby suggesting that the thickness of the film has yet to be optimised. A similar trend was observed for electrodes annealed for 30 min for each layer.

The effect of annealing temperature on the observed photocurrent can be seen in Fig. 7. A typical dark current for these electrodes in shown in Fig. 7(viii).

Here, each electrode consisted of 6 layers and annealed for 10 min for each layer. It can be seen that there is a clear increase in photocurrent with annealing temperature. Perhaps predictably, electrodes which were found to be predominantly amorphous (those annealed below 450 °C) were found to give negligible photocurrents. As the thin film of photocatalyst crystallises, the photocurrent increased with the largest current density being *ca.* 90 μA cm$^{-2}$ at 0.53 V *vs.* SCE for an electrode annealed at 700 °C. The increase in photocurrent is suggested to be due to the increase in crystallinity as observed in the Raman and SEM analysis. These photocurrents densities are low when compared to established photoelectrodes such as $WO_3$ (*ca.* 1.6 mA cm$^{-2}$) [8] or $Fe_2O_3$

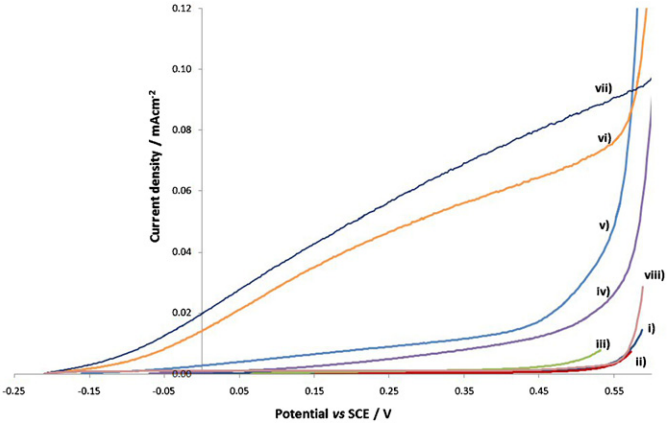


**Fig. 7.** Photocurrent–voltage plots for iron vanadate electrodes consisting of 6 layers. Electrodes annealed at: (i) 250 °C; (ii) 350 °C; (iii) 450 °C; (iv) 550 °C; (v) 600 °C; (vi) 650 °C; and (vii) 700 °C. The corresponding dark current is given in (viii).

($600\,\mu A\,cm^{-2}$) [6], however work is ongoing to develop Fe–V–O systems to increase their photoresponse.

## 4. Conclusions

Iron vanadate has been prepared from a low-temperature, aqueous solution–precipitation reaction. The resulting powder was found to be largely amorphous and required a subsequent annealing step to induce crystallinity. Annealing at temperatures below 450 °C typically afforded amorphous material with a particle size in the range 50–80 nm. As the annealing temperature increased, the crystallinity of the powder increased concomitantly. For powder samples annealed above 550 °C, crystalline triclinic $FeVO_4$ was found. The extent of crystallinity increased further when annealed above 600 °C and the presence of hematite was observed. Particle sizes increased to 100 nm. Band gaps were found to be *ca.* 2.00 eV and it is suggested that this is due to an indirect transition. Photoelectrochemical measurements under simulated solar illumination showed that iron vanadate photoanodes afforded a measurable photocurrent which increased with the number of layers deposited and the annealing temperature.

## Appendix A. Supplementary data

Supplementary data associated with this article can be found, in the online version, at doi:10.1016/j.jphotochem.2010.08.010.

## References

[1] R. van der Krol, Y. Liang, J. Schoonman, J. Mater. Chem. 18 (2008) 2311–2320.
[2] N.S. Lewis, D.G. Nocera, PNAS 103 (2006) 15729–15735.
[3] A. Fujishima, K. Honda, Nature 238 (1972) 37–38.
[4] F.E. Osterloh, Chem. Mater. 20 (2008) 35–54.
[5] B.D. Alexander, P.J. Kulesza, I. Rutkowska, R. Solarska, J. Augustynski, J. Mater. Chem. 18 (2008) 2298–2303.
[6] A.A. Tahir, K.G.U. Wijayantha, S. Saremi-Yarahmadi, M. Mazhar, V. McKee, Chem. Mater. 21 (2009) 3763–3772.
[7] C. Jorand Sartoretti, B.D. Alexander, R. Solarska, I. Rutkowska, J. Augustynski, R. Cerny, J. Phys. Chem. B 109 (2005) 13685–13692.
[8] C. Santato, M. Odziemkowski, M. Ulmann, J. Augustynski, J. Am. Chem. Soc. 123 (2001) 10639–10649.
[9] K. Sayama, A. Nomura, T. Arai, T. Sugita, R. Abe, M. Yanagida, T. Oi, Y. Iwasaki, Y. Abe, H. Sugihara, J. Phys. Chem. B 110 (2006) 11352–11360.
[10] S.S. Dunkle, R.J. Helmich, K.S. Suslick, J. Phys. Chem. C 113 (2009) 11980–11983.
[11] G.S. Li, D.Q. Zhang, J.C. Yu, Chem. Mater. 20 (2008) 3983–3992.
[12] C.S. Enache, D. Lloyd, M.R. Damen, J. Schoonman, R. van de Krol, J. Phys. Chem. C 113 (2009) 19351–19360.
[13] T. Arai, Y. Konishi, Y. Iwasaki, H. Sugihara, K. Sayama, J. Comb. Chem. 9 (2007) 574–581.
[14] K. Melghit, A.S. Al-Mungi, Mater. Sci. Eng. B 136 (2007) 177–181.
[15] J. Deng, J. Jiang, Y. Zhang, X. Lin, C. Du, Y. Xiong, Appl. Catal. B 84 (2008) 468–473.
[16] P. Poizot, E. Baudrin, S. Laruelle, L. Dupont, M. Touboul, J.-M. Tarascon, Solid State Ionics 138 (2000) 31–40.
[17] S. Bencic, B. Orel, A. Surca, U.L. Stangar, Sol. Energy 68 (2000) 499–515.
[18] Z. He, J. Yamaura, Y. Ueda, J. Solid State Chem. 181 (2008) 2346–2349.
[19] A. Galembeck, O.L. Alves, Thin Solid Films 365 (2000) 90–93.
[20] A.Š. Vuk, B. Orel, G. Dražič, F. Decker, P. Colomban, J. Sol-Gel Sci. Technol. 23 (2002) 165–181.
[21] M. Nohair, D. Aymes, P. Perriat, B. Gillot, Vib. Spectrosc. 9 (1995) 181–190.
[22] D.L.A. de Faria, S.V. Silva, M.T.D. Oliveira, J. Raman Spectrosc. 28 (1997) 873–878.
[23] A. Murphy, Sol. Energy Mater. Sol. Cells 91 (2007) 1326–1337.
[24] J. Tauc, R. Grigorovici, A. Vancu, Phys. Status Solidi B 15 (1966) 627–637.
[25] J. Luan, B. Pan, Y. Paz, Y. Li, X. Wu, Z. Zou, Phys. Chem. Chem. Phys. 11 (2009) 6289.
[26] W. Tong, L. Li, W. Hu, T. Yan, G. Li, J. Phys. Chem. C 114 (2010) 1512–1519.
[27] C. Jorand Sartoretti, M. Ulmann, B.D. Alexander, J. Augustynski, A. Weidenkaff, Chem. Phys. Lett. 376 (2003) 194–200.